Non-linear transport and structure formation in semi-insulating GaAs

1996 J. Phys.: Condens. Matter 8 7493

(http://iopscience.iop.org/0953-8984/8/40/013)

J. Phys.: Condens. Matter **8** (1996) 7493–7508. Printed in the UK

Non-linear transport and structure formation in semi-insulating GaAs

B Willing† and J C Maan‡

† Grenoble High Magnetic Field Laboratory, Max-Planck-Institut für Festkörperforschung, 25 Avenue des Martyrs, F-38042 Grenoble, France

‡ High Field Magnet Laboratory, Research Institute for Materials, University of Nijmegen, NL-6525 ED Nijmegen, The Netherlands

Received 15 March 1996, in final form 26 June 1996

Abstract. We present an experimental study of slow domains in semi-insulating GaAs using time-resolved, two-dimensional electro-optic voltage probing. A detailed analysis of the shape of the bulk domains proves that they are formed by symmetric charge dipoles made up from ionized traps. The study of the dependence of the domain parameters on the applied voltage allows us for the first time to reconstruct experimentally the bulk $j(E)$-characteristic of SI-GaAs and to show that prevailing theoretical models fail to explain the observations. The experimentally determined field dependence of the free-carrier concentration reveals a strongly field-enhanced trapping with no critical field. The drift velocity of domains is experimentally found to be exclusively determined by the free-carrier concentration at the centre of the domain.

1. Introduction

This paper describes an experimental study of the strongly non-linear conductivity in semi-insulating (SI-) GaAs at high electric fields. Under these conditions, a decrease in the current density above a threshold field is observed which is caused by the spontaneous partition of a sample into low-field regions and a high-field domain (figure 1). This domain drifts through the sample, leading to an oscillation of the total current under constant applied voltage. A system showing such a structure formation cannot be described by a 'bulk conductivity', and measurements of current and voltage at the end contacts will only provide very limited information. We here present experimental data obtained with a set-up that can measure quantitatively the local voltage distribution in the sample with a high spatial and temporal resolution.

The best known example of domain formation in GaAs n-type samples [1, 2] is the Gunn effect, where negative differential conductivity (NDC) is caused by scattering of conduction electrons into a band of higher effective mass [3, 4]. However, in the 1960s another very different type of domain was found in SI-GaAs [5, 6], with drift velocities about six orders of magnitude lower and an estimated critical field for the onset of domains being reported to be approximately three times lower than the one for the Gunn effect ($E_{c,Gunn} = 3.1 \times 10^5$ V m^{-1}). Successive experimental work during the following 15 years led to the development of a theory based on field-enhanced trapping of electrons in a deep level [7, 8]. In the 1980s these slow domains saw a revival of interest when several groups were able to demonstrate routes to chaos in the oscillations of a SI-GaAs sample [9–13].

0953-8984/96/407493+16$19.50

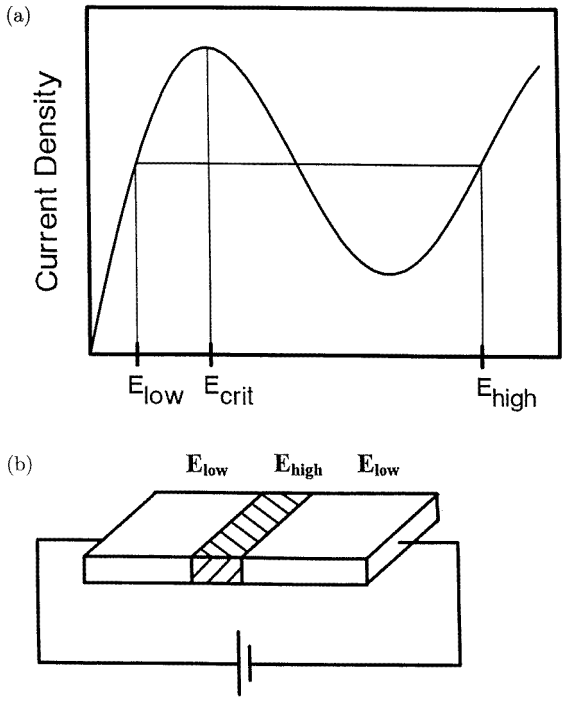

Figure 1. A schematic non-linear $j(E)$-characteristic with an N-shaped negative differential conductivity (a) which leads to the topological partition of a sample into domains (b).

Although the model of field-enhanced trapping has been commonly accepted, it was never tested experimentally in any detail as no spatially resolved measurements of voltages were available. Apart from purely qualitative imaging methods [14–16], experiments so far have only measured the total current and voltages, partly in connection with a spatially resolved light irradiation technique [17]. In this work, we apply an electro-optic technique derived from the spot-like voltage-probing technique originally developed by Fontein *et al* [18] which enables one to look 'into the sample' and to measure quantitatively the time-resolved, two-dimensional voltage distribution in a non-invasive manner. Clearly, these experiments provide much more detailed information about domain formation than earlier reports. This information can be used to assess critically prevailing theoretical models and to conclude that these are in disagreement with the experimental observation in several respects.

This paper is organized as follows. In the next section, the experimental set-up is described; this description is followed by a brief outline of the general behaviour of the transport in SI-GaAs at high fields. In the third section, experimental results on the propagation of stable domains in the bulk are presented, and the quantitative measurements of local voltage distributions $V(x, y, t)$ give direct access to the non-linear properties of bulk SI-GaAs. The analysis of the growth of domains with bias allows us to reconstruct the underlying bulk SI-GaAs $j(E)$-characteristic experimentally which, due to the lack of spatially resolved measurements, had not been available up to now. The data provide the intrinsic non-linearity of the free-carrier concentration n_{free} as a function of the electric field, from which we can determine the field dependence of the net capture coefficient $c(E)$

of the related deep traps. This experimentally determined field dependence is found to be responsible for the main discrepancies between the existing models for slow domains and the experimental facts.

2. Experimental aspects

The experimental set-up to measuring the two-dimensional voltage distribution of a sample with high temporal resolution is based on the electro-optic effect which transfers the potential distribution of the sample into a phase-shift distribution of light via an electro-optically active crystal. A polarized, collimated laser beam illuminates the crystal which is placed on top of the sample, and the light reflected from the sample–crystal interface is observed by a fast CCD camera through a crossed analyser. For any given time, the local voltages can be extracted from the displayed light intensity distributions.

Because of the Pockels effect (linear-electric-field-induced birefringence) in electro-optic crystals, a beam of light transmitted through the crystal experiences different velocities on mutually perpendicular axes of polarization, resulting in a change Γ of the polarization of the light. We use as the electro-optic crystal the bismuth silicate $Bi_{12}SiO_{20}$ (BSO) of the 23 symmetry group in the longitudinal configuration (that is, with the propagation vector of light parallel to the direction of the electric field). The phase shift Γ of the polarization between incoming and outcoming light is given by [21]

$$\Gamma = \frac{2\pi}{\lambda} k_0^3 r_{41} E d = \pi \frac{V}{V_\pi} \tag{1}$$

where d is the thickness of the crystal, λ the wavelength of the light, k_0 the index of refraction and r_{41} the electro-optic coefficient of BSO. V is the voltage drop across the thickness d, and V_π is the (material-dependent) voltage required to introduce a phase shift of π. Using circularly polarized light, the intensity ratio of incoming and outcoming light with the electro-optic crystal observed through a linear polarizer is

$$\frac{I_{out}}{I_{in}} = \frac{1}{2}\left[1 + \sin\left(\pi \frac{V}{V_\pi}\right)\right]. \tag{2}$$

The BSO ($10 \times 10 \times 5$ mm^3) is cut normal to the $\langle 100 \rangle$ direction. One of the surfaces is furnished with an anti-reflective coating of which the outmost layer is an indium tin oxide (ITO) deposit serving as a transparent electrode. Onto the opposite side, a dielectric mirror is deposited; this prevents the light from entering the sample. The BSO is placed with its dielectric mirror onto the surface of the sample and the ITO electrode is connected to a fixed potential with respect to the sample (i.e. $V_{ITO} = 0.5 V_{appl}$), thus creating a reference potential plane. Any voltage distribution $V_{sample}(x, y)$ is thereby translated into an electric field distribution $E(x, y)$ along the z-direction of the BSO and is read out via the electro-optic effect. To avoid convection of air and to allow for precise temperature control, the BSO was mounted on the sample within a closed cell.

A semiconductor laser diode with a wavelength of $\lambda = 780$ nm was used as the light source. Its beam is brought into a square shape of 10×10 mm^2) before passing a linear polarizer and a quarter-wave plate. After reflection at the dielectric mirror, the beam is coupled by a 50% beam splitter through a crossed analyser into the aperture of a CCD camera. The CCD camera has an output frame of 512×512 8-bit pixels and can be operated asynchronously with the video mode. Each frame is taken over by a frame-grabber board implemented in a standard personal computer. The camera and frame grabber are triggered at fixed moments of the domain cycle by means of a signal derived from the

current pulses of the sample. To avoid speckle patterns in the images, the laser is triggered to give two or three independent pulses (with independent speckle patterns) during each exposure of a frame. An average over 256 frames is taken of the same event and the result is put into a 16-bit-deep frame. This routine significantly enhances the signal-to-noise ratio and allows a scaling of intensities better than the 8 bit of the camera. Calibration is achieved by putting the sample at a uniform potential with respect to the BSO electrode and recording the intensity distribution. The frame is normalized pixel to pixel to a frame taken at zero potential. Repeating this procedure subsequently for various voltage steps, one obtains a set of calibration frames containing the desired information. In the experiment, the homogeneous potential is replaced by the actual voltage distribution and each measurement frame is normalized to $I_{in}(x, y)$ by the same operation as for the according calibration frames. We obtain an absolute voltage resolution of $\Delta(V - 0.5V_{appl}) = 10$–$15$ V which corresponds to 5–1% of the applied voltages in the range of interest of V_{appl} of 200–2500 V.

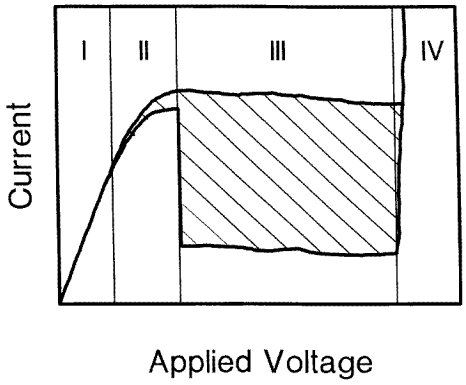

Figure 2. A typical $I(V_{appl})$-characteristic of a sample, showing four different regimes: I, ohmic; II, small sinusoidal oscillations; III, large pulse-like oscillations; IV, electrical breakdown. The upper and lower curves represent the maximum and minimum current between which the system oscillates (hatched area).

The temporal resolution is determined by the minimum exposure window of $\delta t = 50\ \mu$ s which for slow domains with drift velocities of $v_D = 0.001$–0.1 ms^{-1} is more than sufficiently small since the drift of the domain during the exposure is $\delta x \simeq \mu$m.

3. Experimental results

3.1. Samples

All of the samples investigated were prepared from LEC-grown, unintentionally doped single-crystal GaAs wafers (Sumitomo). The low-field mobility is given by Sumitomo as $\mu_0 = 0.5$ m^2 V^{-1} s^{-1}. The density of deep levels (i.e EL2) was not measured, but in this material it is known to be about $n_{EL2} = 2 \times 10^{22}$ m^{-3} [14]. The samples were cut to different sizes, each with a thickness of $d = 0.45$ mm, a width of 5 mm and the sides in the $\langle 100 \rangle$ direction. The contacts were parallel stripes with spacings of $L = 4$–7 mm. They were made of a eutectic alloy of Au/Ge containing 6% Ni and were annealed for 10 min at 420 °C under an inertial gas atmosphere.

Figure 2 shows a typical current–voltage ($I(V_{appl})$-) characteristic obtained for all samples, which is similar to those reported in the literature [22, 10, 23, 16, 24, 25]. With

increasing applied voltage V_{appl}, both the total current and the optically observed real-time voltage distribution show four distinct subsequent regimes (see also [19]). After an ohmic regime (I), small sinusoidal oscillations with frequencies of 1–100 Hz appear in the dc component of the current which correspond to weak domains propagating as fluctuations of the field within the cathode region (II). Above a critical field of $E_c \geqslant 3 \times 10^5$ V m^{-1}, the shape of the current oscillations sharply changes into a pulse-like one and distinct, stable domains form over the whole width of the sample (III). For a wide range of voltages, the current pulses are strictly periodic but become chaotic at high voltages. At very high voltages the current rises by more than three orders of magnitude, leading to the final electric breakdown of the sample, usually accompanied by destruction (IV).

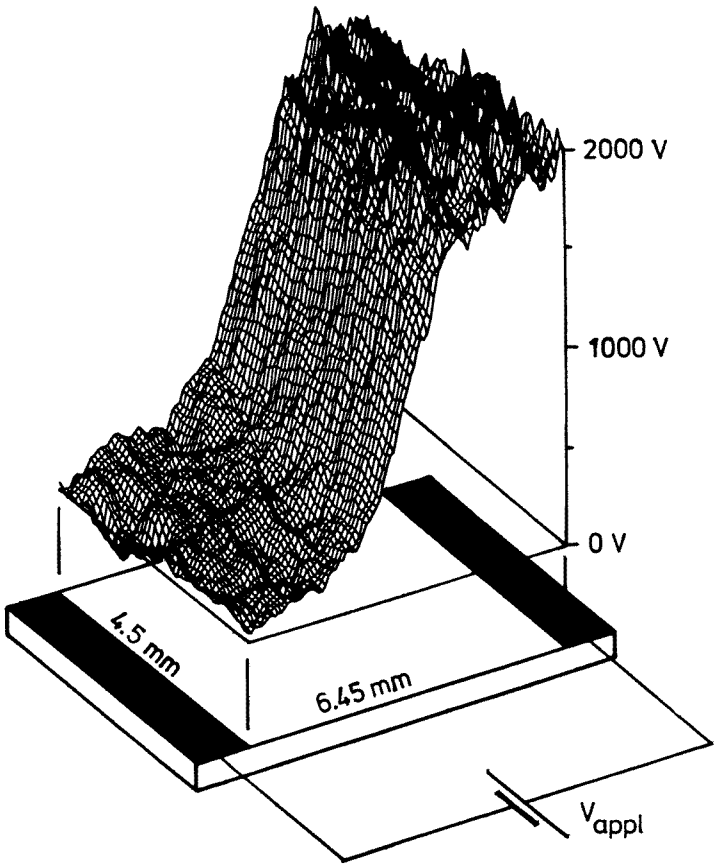

Figure 3. A typical result on the measured voltage distribution in a sample (bottom, with parallel contacts). Almost all voltage drops in the middle of the bulk sample, forming a high-field domain which drifts at $\sim$0.06 m s^{-1} from the left (cathode) to the right (anode). The exposure time of the camera is 50 μs.

3.2. Stable-domain propagation

In this paper we concentrate on part III of the $I(V_{appl})$-characteristic and investigate the features of stable domains in bulk GaAs. In a previous paper we have shown [19] that as

soon as the domain leaves the contact region and enters the bulk sample, its characteristic properties are entirely determined by the bulk parameters. Under these conditions, we use quantitative measurements of the voltage profiles over the domains to obtain detailed information about the bulk non-linear conductivity. The study of the growth and the shape of domains as functions of the applied voltage gives new insight into the basic non-linearities such as the free-carrier concentration $n_{free}(E)$ and net capture coefficient $c(E)$ of the traps. Experiments were performed on three different bar-shaped samples with contact spacings of $L = 6.45$ mm (A), $L = 4.05$ mm (B) and $L = 4.25$ mm (C). The voltage distribution over a sample was measured at a time when the domain was about in the middle of the sample in order to eliminate any residual influence of the contacts. For the same reason, experiments were done for both directions of V_{appl}, each contact acting as the cathode part of the time. Because of the synchronous exposure technique, the domains could only be measured within a range of V_{appl} where the domain cycle is strictly periodic. Figure 3 shows a typical voltage profile obtained for sample A from which we directly extract the domain width w as the distance between 10% and 90% of the voltage drop over the domain. Differentiation of the profile gives the field distribution $E(x)$ including the peak domain field E_{peak} and the field far from the domain E_{out}, and the space-charge profile $\rho(x)$. It can be seen in figure 3 that in general w is not small compared to the length of the sample, so E_{out} can only be estimated as $E(x)$ steadily decreases towards the contacts.

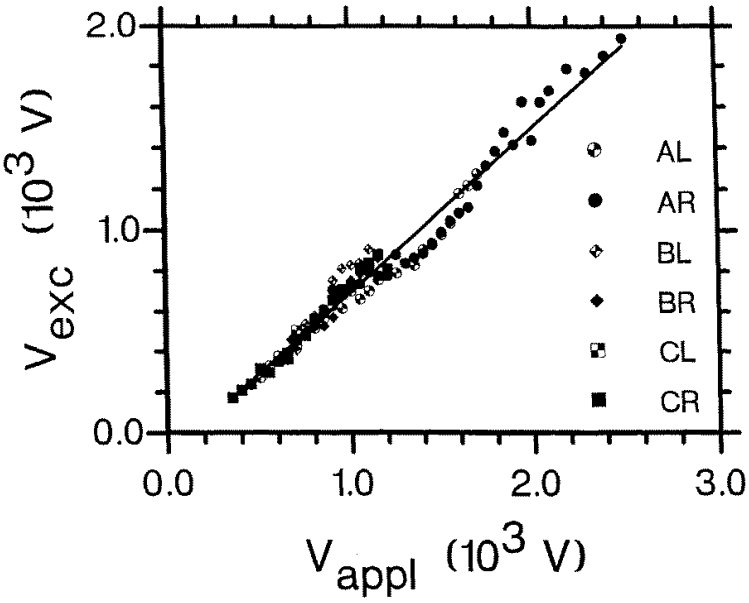

Figure 4. The domain size V_{exc} as a function of the applied voltage V_{appl} for samples A, B and C, with either the left (L) or the right (R) contact as the cathode.

In order to proceed it is necessary to establish a measure for domains which is independent of the specific sample. V_{appl} is related to the contact spacing and can thus not be used for this purpose. A possible characterization of a domain is in terms of its

excess voltage V_{exc} which is defined for a finite sample by [7]

$$V_{exc} = \int_{x=0}^{L} [E(x) - E_{out}]\,\mathrm{d}x \approx V_{appl} - E_{out}L. \tag{3}$$

V_{exc} is a normalization of V_{appl} to the sample length and can be pictured in an $E(x)$-plot as the area under the electric field of a domain which exceeds the level of E_{out}. Being a simple measure of the overall domain size, it gives no further details on the domain's width or peak field.

We determined V_{exc} directly from the voltage profiles by means of the slopes of $V(x)$ in the centre of the domain, near the cathode and near the anode. As seen in figure 4, the domain size as a function of the applied voltage $V_{exc}(V_{appl})$ shows the same dependence for all samples and shows no influence of the actual cathode. Furthermore, V_{exc} does not saturate in the range, 350 V $\leqslant V_{appl} \leqslant$ 2500 V, of stable-domain cycles investigated. We can therefore conclude that V_{exc} reflects an intrinsic bulk SI-GaAs property and that it can be used as a sample-independent parameter for domains.

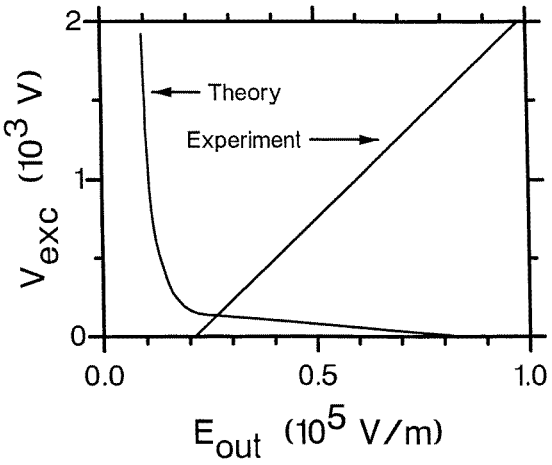

Figure 5. A comparison between $V_{exc}(E_{out})$ predicted by theory (for a carrier concentration of $n_0 = 5 \times 10^{14}$ m^{-3}, after Sacks and Milnes [7]) and the result obtained by the experiment.

The basic relationship between V_{appl} and V_{exc} already allows one to derive the general shape of the $j(E)$-characteristic. We analyse the reaction of the low-field region (E_{out}) to an increase of the domain size V_{exc} by fitting the data of figure 4 to

$$V_{exc} = -b_0 + b_1 V_{appl} \tag{4}$$

where b_1 is a parameter determining the size of a domain as a function of the applied voltage. Comparing equation (4) to the definition of V_{exc} (equation (3)) gives

$$E_{out} = \frac{b_0}{L} + \frac{1 - b_1}{b_1 L}(V_{exc} + b_0). \tag{5}$$

Obviously, b_1 has a critical value $b_1 = 1$, since for $b_1 > 1$, E_{out} has to decrease with increasing V_{exc} while for $b_1 < 1$, E_{out} increases. Since we find for all of the samples the same value of $b_1 = 0.8 \pm 0.1$, it is a parameter specific to SI-GaAs and not to a particular sample. As b_1 is smaller than unity, we can state that the outside field increases with increasing V_{exc} and, consequently, the low-field regions and the domain are *both* operated

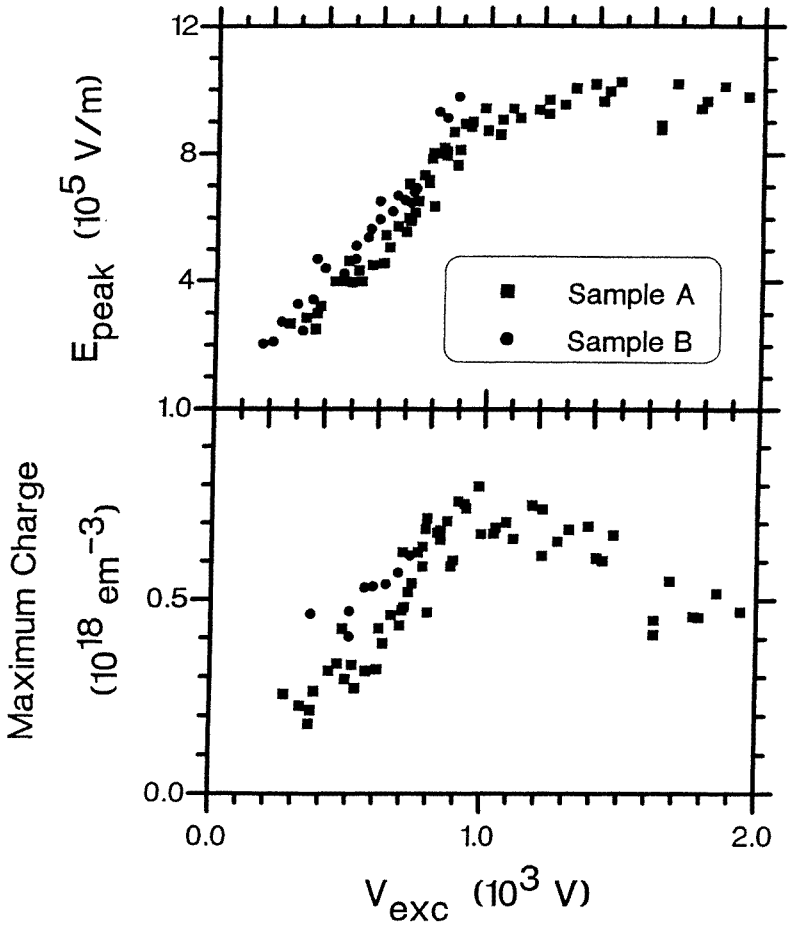

Figure 6. The maximum electric field E_{peak} and maximum space charge of domains as functions of V_{exc} for samples A and B.

on stable branches (i.e. with $\mathrm{d}j/\mathrm{d}E > 0$) of $j(E)$. The latter has therefore to be composed within the range ($0 \leqslant E \leqslant 11 \times 10^5$ V m^{-1}) investigated: a stable low-field regime, an unstable intermediate regime and a stable high-field branch (N-shaped; see figure 1).

This is fundamentally different from the case of Gunn domains of which the domain peak field coincides with the central, unstable intersection. On the basis of theoretical modelling it has been argued [7] that the structural growth of domains in SI-GaAs would follow the mechanism of Gunn domains. In this model, an increase of the domain (in both V_{exc} and the domain peak field) would be associated with a decrease of the stable field outside of the domain (figure 5), but our data show very clearly that this conjecture does not hold.

We now turn to a more detailed investigation of domains in order to obtain information about the space charge involved. A first general observation is that independently of its size, the electric field profile of a domain is symmetrical as already predicted [7, 8]. Figure 6 (upper panel) shows that E_{peak} grows linearly with V_{exc} up to $V_{exc} \cong 1000$ V where it saturates at a value of $E_{peak} \cong 10 \times 10^5$ V m^{-1}. This implies that the total amount

of charge (ionized traps and/or free carriers) accumulated in a domain is limited.

The dipole peak value $|\rho/e|_{max} = (|\rho_{max,-}| + |\rho_{max,+}|)/2e$ grows linearly with V_{exc} (figure 6 (lower panel)) and reaches a maximum at about the same domain size as that at which E_{peak} saturates, before it decreases further. The maximum value of the charge density forming the domain, $\rho \cong 0.8 \times 10^{18}\ e\ \mathrm{m}^{-3}$, is a factor of 10^5 higher than the free-carrier concentration. Therefore, the space charge of the domains has to involve mainly localized charge density on traps; and figure 6 (lower panel) represents a plot of this charge as a function of V_{exc}. Apparently, there is a mechanism which limits the ionization of traps, because their total density is of the order of $10^{22}\ \mathrm{m}^{-3}$ whereas the maximum detected charge density corresponds to only 0.01% of this trap density.

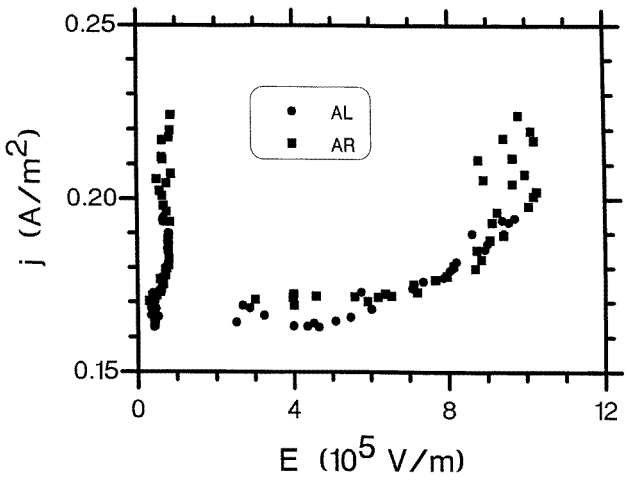

Figure 7. The bulk $j(E)$-characteristic measured for sample A.

This localized space charge is a second basic difference from the case of Gunn domains which are entirely formed by a modulation of the free-carrier concentration and are highly asymmetrical in shape. Our space charge profiles (figure 9 (lower panel); see below) clearly show that the domain is built up of a symmetric amount of negative and positive space charge whereof the latter cannot be explained by a trapping of electrons. Without a detailed knowledge about the rather complicated trap composition in this material [29], we will refer later to a net capture coefficient $c(E)$ for SI-GaAs. In this picture, the capture mechanism gives the accumulation of the negative space charge at the leading edge of the domain. The trailing edge's positive space charge should occur due to a local distortion of the band structure by the huge negative charge which in turn affects the occupation of the present shallow donors.

On the basis of our experimental results, we can derive important information about the intrinsic non-linear parameters of SI-GaAs. Since we know the general shape of $j(E)$ with two stable branches, and that the current density through the sample is governed by the domain peak field E_{peak} [19], we can construct the two stable points of the $j(E)$-characteristic. They are given by $(I/A)(E_{peak})$ and $(I/A)(E_{out})$, where I is the laterally homogeneous total current through the sample's constant cross-section A. Figure 7 shows $j(E)$ as obtained by taking successive voltage profiles for sample A and represents the first direct, experimental measurement of the real bulk $j(E)$-characteristic of this system so far. However, it should be noted that $j(E)$ is a local characteristic which may vary with the

local defect and impurity concentration, whereas our values of E_{peak} and E_{out} are taken on two different locations of the sample. Figure 7 therefore represents an average of $j(E)$ over the sample.

The electric field value of the low-field maximum of the current density in figure 7 should not be confused with the critical fields directly measured in [19]. Taken from voltage profiles of stable domains, the $j(E)$ presented here includes only points at which the electric field is stable and has to leave out any parts of the characteristic which are unstable or critical. The argument that relevant information could be obtained from the maximum current I_{peak} arising from the annihilation of the domains during a cycle does not hold because this value is entirely determined by contact properties [19, 20].

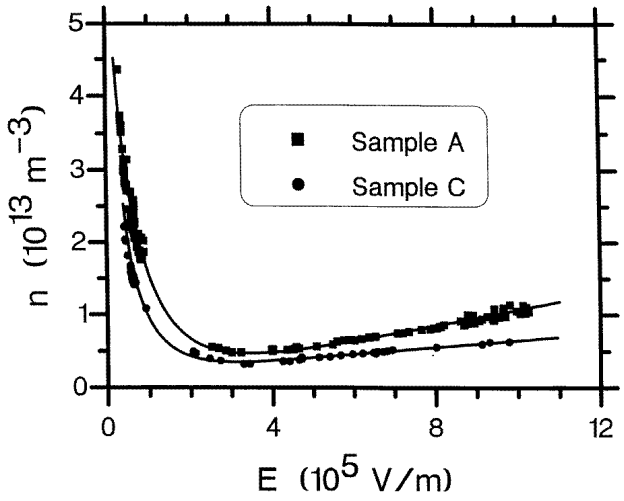

Figure 8. The free-carrier concentration n_{free} as a function of the electric field for samples A and C, obtained from the analysis of the experimental data. The solid curves represent an empirical fit.

Figure 7 and figure 6 (upper panel) explain the high-field limits for the existence of stable, periodically oscillating domains. Upon increasing V_{exc}, E_{peak} for a medium-sized domain increases and, simultaneously, both j_{min} and E_{out} increase according to the $j(E)$-curve. With E_{peak} saturating at a certain value of V_{exc}, the domain becomes wider rather than higher and the current increases drastically. This leads to a forced increase of E_{out} and eventually to a state where even the low-field regions become critical: the sample is at the edge of stability for domains. Although the details of this second transition are not clear, it is consistent with our observation that from certain values of V_{exc} on, the period of a domain cycle becomes irregular.

Using the relation $j(E) = en_{free}(E)\mu(E)E$, we can obtain the free-carrier concentration $n_{free}(E)$ by eliminating the well known carrier mobility $\mu(E)$ [26]. Although this mobility may vary in amplitude between different samples, we assume that its shape as a function of field does not change under variations of the impurity concentration. Figure 8 shows the $n_{free}(E)$-characteristics for the samples A and C, both revealing the same dependence. The absolute value of $n_{free}(E) = \mathrm{O}(10^{13}\ \mathrm{m}^{-3})$ is in good agreement with the data provided by the wafer manufacturer and variations should be due to variations of the impurity and trap concentration. n_{free} decreases roughly exponentially for fields below 1×10^5 V m^{-1}, reaching a minimum at around $E = 3 \times 10^5$ V m^{-1} and increasing linearly with higher

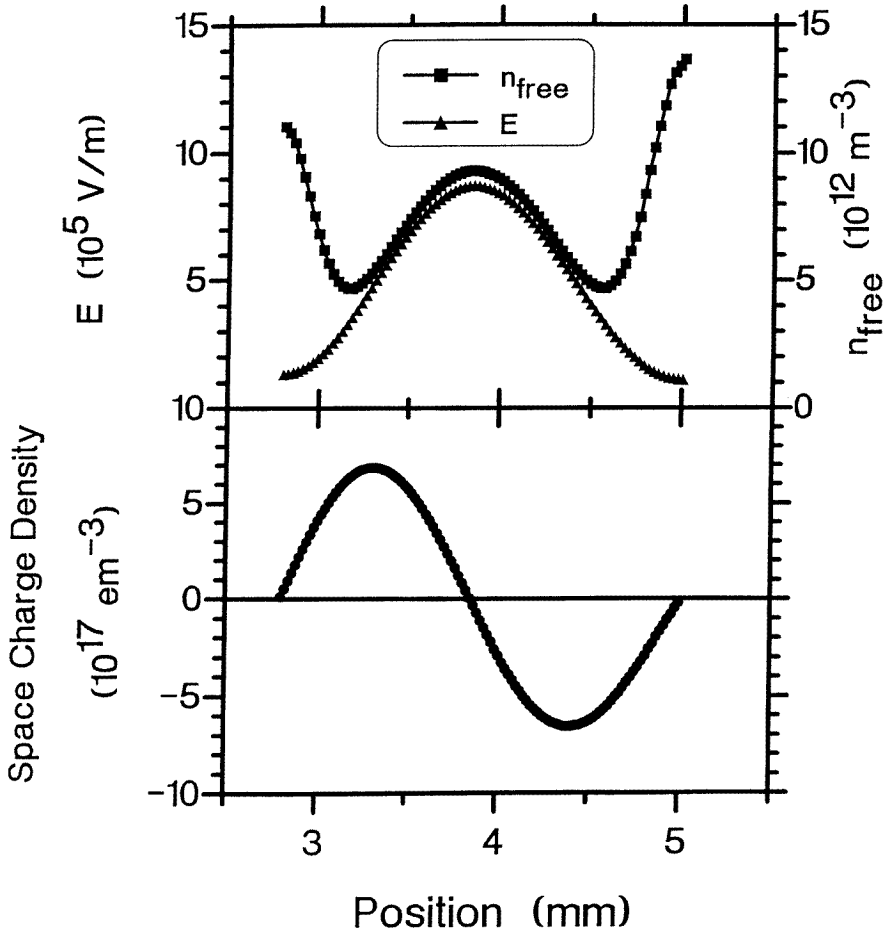

Figure 9. $E(x)$ and $n_{free}(x)$, together with the space-charge density, for a domain at $V_{exc} = 1000$ V ($L = 6.45$ mm). Note the small fraction of free carriers with respect to the charge density.

fields. This exponential decrease is consistent with a trapping mechanism over a repulsive barrier, but so far we have not observed the corresponding critical field for the onset of the decrease of n_{free}. This first experimental determination of $n_{free}(E)$ has only been possible due to the spatially resolved measurement of a stable structure.

The free-carrier profile of a domain calculated from a combination of the experimental data $E(x)$ and $n_{free}(E)$ is shown in figure 9 (upper panel), together with the charge-density distribution $\rho/e(x)$ (corresponding to the distribution of ionized traps $N_{t^-}(x)$) (figure 9 (lower panel)). Due to the minimum of n_{free} at a field of $E \cong 3 \times 10^5$ V m^{-1}, the free-carrier profile has a distinct 'w' shape, recovering towards the centre of the domain to about $\frac{1}{2}n_0$. The charge dipole forming the domain is obviously accompanied by two separated depletion regions of free carriers, whereby the junction represents an almost low-field concentration of carriers. Although the space charge integrated over the whole sample vanishes, a domain clearly represents electronic transport where the local charge neutrality is not given.

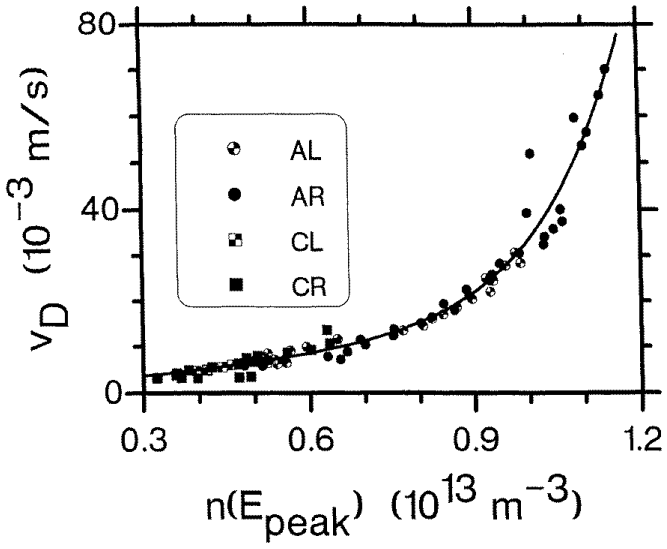

Figure 10. The drift velocity of the domains as a function of the free-carrier concentration at the domain peak field for samples A and C. The solid line represents an empirical fit to $v_D = a_1 n_{free} + a_2 \exp(a_3 n_{free})$ where $a_1 = 1.12 \times 10^{-15}$ m^4 s^{-1}, $a_2 = 3.89 \times 10^{-5}$ m s^{-1} and $a_3 = 6.36 \times 10^{-13}$ m^3.

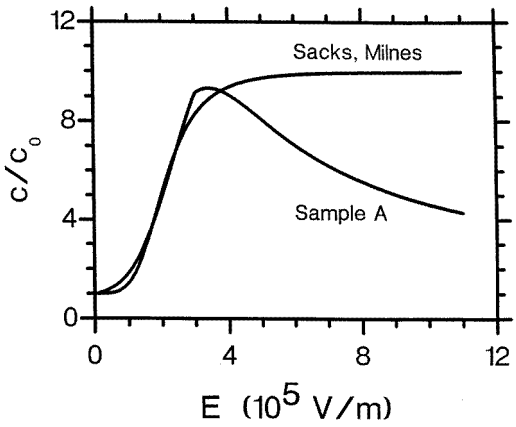

Figure 11. The experimentally determined field dependence of the net capture coefficient $c(E)$ (normalized to $c(E = 0)$) of SI-GaAs and the one assumed by Sacks and Milnes [7].

A final experimental result concerns the drift velocity v_D of the domains which is found to be given for all samples by the free-carrier concentration at the centre of the domain $n_{free}(E_{peak})$ (figure 10). This observation contrasts with previous speculations, stating that the domain velocity scales with the free-carrier velocity reduced by the ratio of the low-field carrier concentration and the ionized traps n_0/N_{t^-}. Although this conjecture gives the right order of magnitude for v_D, and the dependence $v_D \sim n_0$ was confirmed by a number of other workers [9, 22, 15], the relation $v_D \sim 1/N_{t^-}$ is incompatible with our more detailed data. Figure 6 (lower panel) shows that N_{t^-} first increases and then decreases with domain size

while the velocity increases steadily. To understand the dependence of v_D on $n_{free}(E_{peak})$, a closer analysis of the mechanism determining the drift velocity of a domain has to be performed.

We can use our experimental results in order to determine the field dependence of the capture coefficient of the traps. This dependence is the most important non-linearity as it lies at the very origin of the phenomenon of 'slow domains'. For a stationary state, without net carrier generation and with zero current divergence, the relevant rate equation is given by

$$gN_{t^-}(E) = c(E)n_{free}(E)\,[N_t - N_{t^-}(E)] \tag{6}$$

where the generation rate g is known to be field independent [27]. We know from our measurement that $N_{t^-}/N_t(E) \leqslant 10^{-4} \ll 1$ which, together with $c(E) = c_0 c(E)$, yields

$$c^*(E) = \frac{g}{c_0 n_{free}(E)} \frac{N_{t^-}}{N_t}(E). \tag{7}$$

While $n_{free}(E)$ is known from an experimental fit, the ratio

$$\frac{N_{t^-}}{N_t}(E)$$

is not directly obtained from our data. However, by connecting $N_{t^-}(x)$ to $E(x)$ as was done in figure 9 we can make two important statements: firstly, N_{t^-} increases for low fields at least linearly with field; secondly, N_{t^-} has a maximum at $E \approx 3 \times 10^5$ V m^{-1}, but it is not clear whether it decreases or levels out beyond this field. Taking the simplest approach, $N_{t^-}(E) \sim E$ for $E \leqslant 3 \times 10^5$ V m^{-1} and $N_{t^-}(E) =$ constant for $E > 3 \times 10^5$ V m^{-1}, we arrive at a relation for $c(E)$ which is pictured in figure 11, together with the theoretical prediction of Barraud [28] which was used by Sacks and Milnes.

Two main conclusions can be drawn from this figure: for the theoretical prediction as well as for our experimental reconstruction, the maximum variation of c is $c_{max}/c_0 \approx 10$. Furthermore, both relations are in quite good agreement for the low-field range ($E \leqslant 2.5 \times 10^5$ V m^{-1}) although our result reveals an onset of field-enhanced trapping at substantially lower fields than predicted. The second conclusion is that the capture coefficient does not saturate at high fields but *decreases*, showing a maximum at $E \approx 3 \times 10^5$ V m^{-1}. It should be noted here that the assumed field dependence of N_{t^-} is rather conservative and that a decrease of N_{t^-} towards higher fields would yield an even stronger decrease of c with field. This decrease of the capture coefficient is a fundamental difference from previous models and may explain the discrepancies observed between theory and our experimental data.

It is very remarkable that an electric field value of $E \approx 3 \times 10^5$ V m^{-1} is particular in three different respects. Firstly, it is the critical field for onset of the Gunn effect which causes the scattering of free carriers from the Γ minimum of the conduction band to the higher-lying X minimum of a sub-band with a higher effective mass. The latter causes a drastic decrease of the carrier mobility, thereby leading to the formation of Gunn domains. Secondly, our experimental data clearly show that the free-carrier density has a minimum at the same field of $E \approx 3 \times 10^5$ V m^{-1}. Finally, the evaluation of $c(E)$ gives a maximum of the capture coefficient at this particular field value.

4. Discussion

We summarize as follows. In the low-field region up to $E \leqslant 3 \times 10^5$ V m^{-1}, SI-GaAs shows a drastic decrease of the free-carrier concentration with field which is obviously connected to a field-enhanced trapping mechanism (figure 8 and figure 11). This experimental finding

is in good agreement with the basic assumptions of theory, although we do not observe a critical field for this mechanism. However, direct field measurements [19] prove that there is no formation of stable domains below $E \approx 3 \times 10^5$ V m^{-1} as predicted by the models. It should be noted here that these theories were tailored to give critical fields of $E_c = 1 \times 10^5$ V m^{-1} as those had been estimated from the simple expression critical voltage divided by contact spacing. The origin of the field-enhanced trapping still remains one of the main questions. Due to the observed absence of a critical field, it cannot be of a simple Coulombic origin. As we observe the decrease of the carrier density from the lowest detected fields on, the interaction between traps and electric field has to be of a smooth and progressive nature. However, we cannot propose a possible mechanism at the present time.

The experimental fact that at $E \approx 3 \times 10^5$ V m^{-1}, the minimum of the free-carrier concentration coincides with the onset of the electron transfer to the X minimum implies that the capture mechanism of the traps is less efficient for electrons in the sub-band. Since the ratio of the density of carriers in the sub-band to that of those in the conduction band increases with electric field, the total free-carrier density has to increase and the total capture coefficient will decrease as shown by our data. A possible reason for the smaller capture coefficient from the sub-band could be found in the much higher wave vector of these electrons. Here, trapping is connected to the corresponding phonons of a relatively high energy, and a small capture coefficient may therefore indicate a bottleneck for those phonons.

The phenomenon of slow domains in SI-GaAs, as it appears in the light of these new experiments, is based on substantial contributions from two effects. The decrease of the carrier density related to field-enhanced trapping as determined by our measurement alone does not give a NDC region in the $j(E)$-characteristic. The NDC region observed and the critical field of $E_c \approx 3 \times 10^5$ V m^{-1} have therefore to be caused by the additionally acting Gunn effect. On the other hand, in a SI-GaAs sample a domain could not form without field-enhanced trapping because the free-carrier density is far too low to build up the domain's space charge during its transit through the sample [3]. Here, the trapping acts in two ways: Firstly, it causes the drift velocity of a domain to have to adjust to the capture/generation rate of the traps. The domain's transit time through the sample is therefore sufficiently long to allow an initial perturbation to develop into a stable domain in spite of the low influx of free carriers. Secondly, it enables the build-up of a dipole of localized charge whose space charge is by orders of magnitude higher than the one which could be achieved by a simple modulation of the free-carrier density. In total, the particular field dependence of the capture coefficient is responsible for the true N shape of the $j(E)$-characteristic which leads to the fundamental difference from Gunn domains, namely that both parts of the structure are operated on stable regimes of the system.

5. Conclusion

In this paper we have presented new results of an experimental investigation of slow high-field domains in semi-insulating GaAs samples using a contactless, optical voltmeter. This set-up based on non-invasive electro-optic voltage probing is capable of measuring voltage distributions $V(x, y, t)$ of high absolute accuracy with a temporal resolution of microseconds and a lateral one of micrometres.

We established that the domain excess voltage is a suitable material parameter for describing the domains independently of the dimensions of a sample. The analysis of the growth of a domain with this parameter showed that the peak field is limited to $E \approx 10 \times 10^5$ V m^{-1} and that the corresponding, symmetric charge dipole is almost

entirely formed of ionized traps representing at most 0.01% of the total trap concentration.

Our experimental results prove that, contrary to the usual theoretical model, both regions of the sample are operated on stable branches of the $j(E)$-characteristic which therefore has a qualitatively different shape to that proposed theoretically. This knowledge allowed us to obtain the two stable branches of $j(E)$ experimentally. The resulting characteristic provides an explanation for the observed high-field limit of stable domains because eventually even the low-field parts of the sample are driven to instability.

From $j(E)$ we could extract the basic non-linear parameters of the system, namely the free-carrier concentration $n_{free}(E)$ and the net capture coefficient $c(E)$ in SI-GaAs. For fields below $E \approx 3 \times 10^5$ V m^{-1}, n_{free} decreases strongly with field, confirming the concept of field-enhanced trapping. However, the absence of a critical field rules out a simple repulsive barrier. At $E \approx 3 \times 10^5$ V m^{-1} the carrier concentration is at its minimum and increases approximately linearly with field further on. The experimental data showed that a drift velocity of the domains in all samples is proportional to this linearly increasing branch which corresponds to the carrier density at the domain peak field. The empirical model in which the drift velocity is inversely proportional to the density of ionized traps can thus be ruled out.

The field dependence of the net capture coefficient $c(E)$ could be assessed by connecting $n_{free}(E)$ to the principal relation between ionized-trap density and electric field. While its low-field behaviour agrees with the theoretical model, a strong difference from the assumption of a saturation is that the experimental capture coefficient evidently has a maximum at $E \approx 3 \times 10^5$ V m^{-1} and decreases further on. As this maximum coincides with both the critical field for the Gunn effect and the minimum of $n_{free}(E)$, this provides evidence for a smaller capture coefficient for carriers in the X minimum than for those in the Γ minimum.

In summary we have shown that a non-invasive optical voltage probing technique with high temporal and spatial resolution is essential for investigating electronic systems with spontaneous structure formation in any detail. It allowed us for the first time to test the existing theories directly on the basis of experimental data not accessible in the past. The data show that the basic non-linearity giving rise to a critical field is the Gunn effect, but that it is the field-enhanced trapping mechanism which allows the accumulation of space charge and which determines both the dynamics and stability of the domains.

References

[1] Watkins T B and Ridley B K 1961 *Proc. Phys. Soc.* **8** 293
[2] Gunn J B 1963 *Solid State Commun.* **1** 38
[3] Knight B W and Peterson G A 1966 *Phys. Rev.* **147** 617
[4] Knight B W and Peterson G A 1967 *Phys. Rev.* **155** 393
[5] Barraud A 1963 *C. R. Acad. Sci., Paris* **256** 3632
[6] Northrop D C, Thornton P R and Trezise K E 1964 *Solid-State Electron.* **7** 17
[7] Sacks H K and Milnes A G 1970 *Int. J. Electron.* **28** 565
[8] Ridley B K and Wisbey P H 1967 *Br. J. Appl. Phys.* **18** 761
[9] Maracas G N, Porod W, Johnson D A and Ferry D K 1985 *Physica* B **34** 276
[10] Lusakowski J, Jezewski M, Knap W and Kuszko W 1988 *Acta Phys. Pol.* A **73** 183
[11] Pozela J 1981 *Plasma and Current Instabilities in Semiconductors* (Oxford: Pergamon)
[12] Schoell E 1989 *Phys. Scr.* T **29** 152
[13] Shaw M P, Mitin V V, Schoell E and Grubin H L 1992 *The Physics of Instabilities in Solid State Electron Devices* (New York: Plenum)
[14] Maracas G N, Johnson D A, Puechner R A, Edwards J L, Myhajlenko S, Goronkin H and Tsui R 1989 *Solid-State Electron.* **32** 1887

[15] Rajbenbach H, Verdiell J M and Huignard J P 1988 *Appl. Phys. Lett.* **53** 541
[16] Rau U, Peinke J, Parisi J, Karpierz K, Lusakowski J and Knap W 1991 *Phys. Lett.* **152A** 356
[17] Sacks H K and Milnes A G 1971 *Int. J. Electron.* **30** 49
[18] Fontein P F, Hendriks P and Wolter J H 1990 *Surf. Sci.* **229** 47
[19] Willing B and Maan J C 1994 *Phys. Rev.* B **49** 13 995
[20] Willing B 1994 *PhD Thesis* University of Nijmegen, (ISBN 90-9007641-7)
[21] *Piezo-Optic and Related Constants; Landolt–Börnstein New Series* Group III, vol 11 (Berlin: Springer)
[22] Johnson D A, Puechner R A and Maracas G N 1990 *J. Appl. Phys.* **67** 300
[23] Lusakowski J 1990 *Mater. Sci. Eng.* **6** 1
[24] Pozela J, Namajunas A, Tamasevicius A and Ulbikas J 1989 *Appl. Phys.* **48** 181
[25] Derhacobian N and Haegel N M 1991 *Phys. Rev.* B **44** 12 754
[26] Ruch J G and Kino G S 1967 *Appl. Phys. Lett.* **10** 40
[27] Makram-Ebeid S and Lannoo M 1982 *Phys. Rev.* B **25** 6406
[28] Barraud A *PhD Thesis* (Clearinghouse for Scientific and Technical Information, VA 22151, N69-18810-3/26)
[29] Lagowski J, Lin D G, Gatos H C, Parsey J M Jr and Kaminska M 1984 *Appl. Phys. Lett.* **45** 89